ACS APPLIED MATERIALS & INTERFACES

Research Article

www.acsami.org

Nanocasting Technique to Prepare Lotus-leaf-like Superhydrophobic Electroactive Polyimide as Advanced Anticorrosive Coatings

Kung-Chin Chang,[†,‡] Hsin-I Lu,[§] Chih-Wei Peng,[†] Mei-Chun Lai,[†,‡] Sheng-Chieh Hsu,[†] Min-Hsiang Hsu,[†] Yuan-Kai Tsai,[†] Chi-Hao Chang,[†] Wei-I Hung,[†,⊥] Yen Wei,[#] and Jui-Ming Yeh*[,†]

[†]Department of Chemistry and Center for Nanotechnology, [‡]R&D Center for Membrane Technology, [§]Master Program in Nanotechnology and Center for Nanotechnology, Chung-Yuan Christian University (CYCU), Chung Li, Taiwan 32023, Republic of China

[⊥]Institute of Chemistry, Academia Sinica, 128, Section 2, Academia Road, Taipei 115, Taiwan 11529, Republic of China

[#]Department of Chemistry and Key Lab of Organic Optoelectronic & Molecular Engineering of Ministry of Education, Tsinghua University, Beijing 100084, China

ABSTRACT: Nanocasting technique was used to obtain a biomimetic superhydrophobic electroactive polyimide (SEPI) surface structure from a natural *Xanthosoma sagittifolium* leaf. An electroactive polyimide (EPI) was first synthesized through thermal imidization. An impression of the superhydrophobic *Xanthosoma sagittifolium* leaf was then nanocasted onto the surface of the EPI so that the resulting EPI was superhydrophobic and would prevent corrosion. Polydimethylsiloxane (PDMS) was then used as a negative template to transfer the impression of the superhydrophobic surface of the biomimetic EPI onto a cold-rolled steel (CRS) electrode. The superhydrophobic electroactive material could be used as advanced coatings that protect metals against corrosion. The morphology of the surface of the as-synthesized SEPI coating was investigated using scanning electron microscopy (SEM). The surface showed numerous micromastoids, each decorated with many nanowrinkles. The water contact angle (CA) for the SEPI coating was 155°, which was significantly larger than that for the EPI coating (i.e., CA = 87°). The significant increase in the contact angle indicated that the biomimetic morphology effectively repelled water. Potentiodynamic and electrochemical impedance spectroscopic measurements indicated that the SEPI coating offered better protection against corrosion than the EPI coating did.

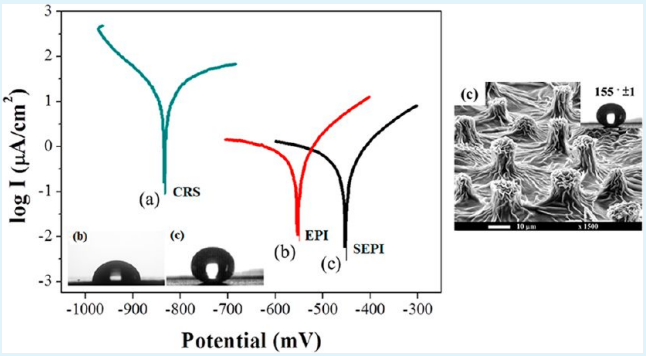

KEYWORDS: *superhydrophobic, electroactive, polyimide, anticorrosion, nanocasting*

INTRODUCTION

Electronically conducting polymers have emerged as a new class of materials in recent decades and have attracted extensive research interest because they exhibit a broad spectrum of potential commercial applications in the electronics, optical, biological, and other civilian/defense industries. Among the conducting polymers, polyaniline (PANI) has great potential for commercial application because of its environmental stability, good processability, and relatively low cost.[1,2] It has previously been reported that PANI could be used to produce electronic devices and products such as anticorrosion coatings,[3−6] batteries,[7−9] sensors,[10,11] separation membranes,[12−14] antistatic coatings,[15,16] electromagnetic interference shielding,[17,18] etc.[19,20] However, PANI prepared using chemical and/or electrochemical means usually exhibits structural defects and has limited solubility in many solvents. These shortcomings would impede better understanding of the structure−property correlations and the conducting mechanism of PANI and thus restrict its practical applications. One possible solution to the problems is to incorporate well-defined and conjugated oligoaniline[21−23] into the copolymer backbones, which could combine the beneficial properties of the specific oligoaniline with the desirable polymer properties such as mechanical strength and film-forming ability.

The availability of oligoanilines enabled us to exploit a variety of potentially electroactive polymers such as polyimides, polyamides, and other derivative polymers. For example, Wang et al. first synthesized and characterized electroactive, high molecular weight, film-forming polyimides derived from the amino-terminated aniline trimer.[24,25] Wei, Zhang et al. subsequently used oxidative coupling polymerization to prepare electroactive polyimide with oligoaniline in the main chain.[26] Incorporating a well-defined oligoaniline into the backbone structure of a conventional polyimide would make it possible to

Received: December 2, 2012
Accepted: February 5, 2013
Published: February 5, 2013

   dx.doi.org/10.1021/am3029377 | ACS Appl. Mater. Interfaces 2013, 5, 1460−1467

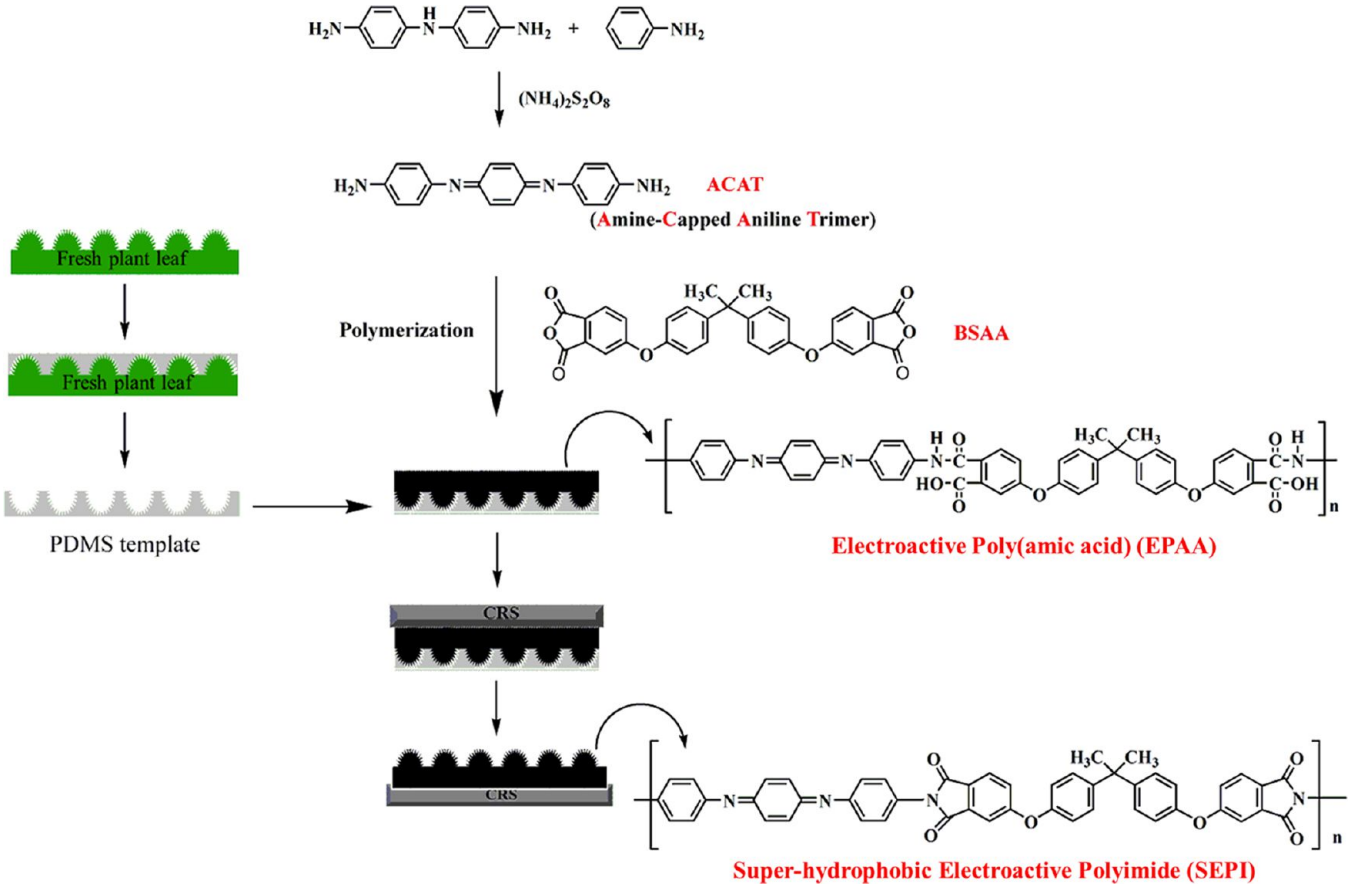

Figure 1. Scheme for using nanocasting technique to prepare biomimetic SEPI coating.

exploit a new electroactive hybrid polyimide, which could exhibits physical properties derived synergistically from both components, such as enhanced electroactivity, mechanical properties and stability at high temperature.

There has recently been intense interest in preparing and studying superhydrophobic surfaces whose water contact angles are larger than 150°. Superhydrophobic surfaces have attracted much attention because of their great potential applications in preventing-snow from adhering to antennas and windows, in self-cleaning traffic indicators, in metal refining, in stain-resistant textiles, etc.[27−31]

Nanocasting,[32] which is based on soft lithography,[33,34] is a method widely used in nanofabrication. The cost of larger scale fabrication is reduced by directly replicating the template to create larger uniform patterns.[35] In this method, a soft, deformable material is used to cast and replicate the structures of the template surfaces. After the soft material solidifies, the complement of the structures on the surface of the original template is transferred to the solidified material. This new template can then be used to repeatedly replicate the surface structures or patterns as long as the template is not factitiously destroyed.

To the best of our knowledge, few studies have previously been done on using electroactive polymers in various applications such as fabricating superhydrophobic surfaces.[36−42]

Therefore, developing superhydrophobic electroactive polymers has become an interesting subject in materials science. In addition, using electroactive polymer coating materials to study the anticorrosive properties that superhydrophobic surfaces convey have rarely been reported to date.[43,44]

In this study, we used nanocasting technique to develop advanced anticorrosion electroactive polyimide (EPI) coatings in order to directly duplicate the surface features of fresh plant leaves such as *Xanthosoma sagittifolium* leaves. The imprint of the superhydrophobic *Xanthosoma sagittifolium* leaf was transferred onto the EPI surface so that the resulting EPI exhibited hydrophobicity to prevent corrosion. The anticorrosion coatings developed in this study also provided 2-fold protection against metal corrosion. The first part of the protection is that the hydrophobicity repelled the moisture and further reduced the amount of water/corrosive media that adsorbed onto the polyimide (PI) surface, preventing the underlying metals from corroding. The second part of the protection is that the electroactive amino-capped aniline trimer (ACAT) component of the developed PI, which can form a passivation oxide layer on the metal surface to prevent the metal surface from further corroding. The detailed anticorrosion performance of the developed EPI coating was evaluated using a series of electrochemical corrosion measurements. Corrosion protection studies were performed on sample-coated cold-rolled steel (CRS) immersed in a corrosive medium (3.5 wt % sodium chloride aqueous solution).

EXPERIMENTAL SECTION

Materials and Instrumental. Aniline (Fluka) was distilled prior to use. 4,4-Diaminodiphenylamine sulfate hydrate (TCI), 4′-(4,4′-isopropylidene-diphenoxy)bis(phthalic anhydride) (BSAA, Aldrich), *N*,*N*-dimethylacetamide (DMAc, Riedel-deHaën), ammonium persulfate (APS, Merck) and polydimethylsiloxane (PDMS, Dow Corning, SYLGARD 184) were used as received without further purification. All reagents were reagent grade, unless otherwise stated.

dx.doi.org/10.1021/am3029377 | *ACS Appl. Mater. Interfaces* 2013, 5, 1460−1467

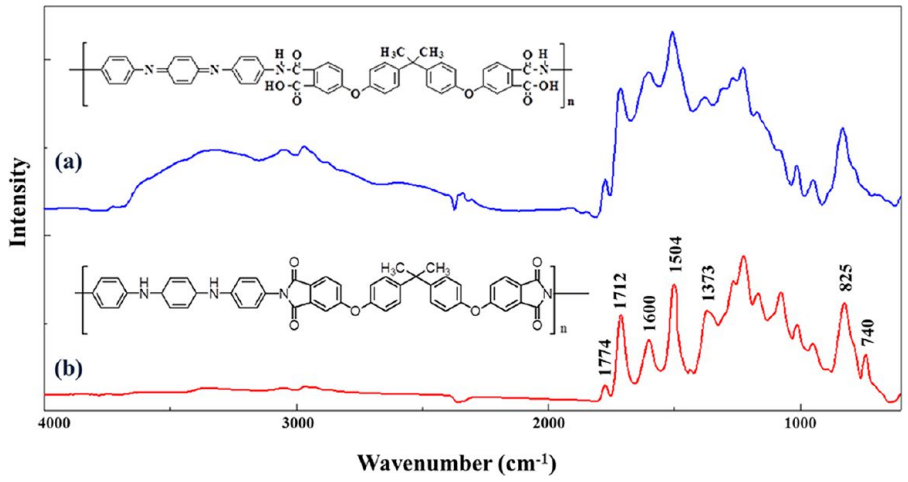

Figure 2. FTIR spectra for (a) EPAA and (b) EPI.

Fourier transform infrared spectra (FTIR) were collected using an FTIR spectrometer (JASCO FT/IR-4100) at room temperature. The morphologies of the surfaces of the coatings and the passivation metal oxide layers were observed using scanning electron microscopy (SEM, Hitachi S-4200). Contact angles were measured using a First Ten Angstroms FTA 125 at ambient temperature. Water droplets (about 4 μL) were carefully dropped onto the surfaces of the samples, and the contact angle was determined from the average of five measurements at various positions on the surfaces of the samples. The corrosion potential and corrosion current of sample-coated cold-rolled steel (CRS) electrodes were electrochemically measured using a VoltaLab 50 potentiostat/galvanostat. Electrochemical impedance spectroscopy (EIS) measurements were recorded on an AutoLab (PGSTAT302N) potentiostat/galvanostat electrochemical analyzer.

Synthesis and Characterization of ACAT. A typical procedure was recently established by Wei et al. for synthesizing ACAT and accordingly, ACAT could be easily synthesized by oxidizing 1,4-phenylenediamine and 2 equiv. of aniline with ammonium persulfate as an oxidant.[45] ACAT is characterized using mass spectrum, FTIR spectrum, and ^{1}H NMR spectrum, which has previously been reported in the literature.[46]

Preparation of PDMS Template. The PDMS prepolymer was obtained by mixing the elastomer base and a curing agent in a proper ratio (10:1, w/w). The PDMS prepolymer was poured into 3 × 6 cm^2 molds fixed to a piece of fresh, natural *Xanthosoma sagittifolium* leaf (The veins of the leaf were removed in an area of about 3 × 6 cm^2.) and then cured in a 60 °C oven for 4 h. After curing, the PDMS blocks were separated from the molds and used as templates for imprinting.

Preparation of Superhydrophobic Electroactive Polyimide (SEPI) Coatings. The electroactive poly(amic acid) (EPAA) was prepared by reacting BSAA with ACAT. The BSAA (0.520 g, 1 mmol) and ACAT (0.288 g, 1 mmol) were separately dissolved in 4.0 g of DMAc. The two solutions were subsequently mixed using a magnetic stirrer for 30 min at room temperature to form EPAA. Drops of EPAA were then spread onto the PDMS template and then the cold-rolled steel (CRS) was pressed against the surfaces of the mixture. The samples were then thermally imidized at 80 °C for 0.5 h, 100 °C for 6 h, 160 °C for 2 h, 200 °C for 2 h, and 30 °C for 6 h. After the thermal imidization reaction, the PMDS template was peeled off from the electroactive polyimide (EPI) coating to obtain the superhydrophobic electroactive polyimide (SEPI) coatings.

Electrochemical Corrosion Studies. The electrochemical corrosion measurements were performed using a VoltaLab 50. All the electrochemical corrosion measurements were also performed at a double-wall jacketed cell, covered with a glass plate, through which water was maintained a constant operational temperature of 25 ± 0.5 °C. The open circuit potential (OCP) at the equilibrium state of the system was recorded as the corrosion potential (E_{corr} in mV versus a saturated calomel electrode (SCE). Tafel plots were obtained by scanning the potential from −500 to 500 mV above E_{corr} at a scan rate of 10 mV/min. The corrosion current (I_{corr}) was determined by superimposing a straight line along the linear portion of the cathodic or anodic curve and extrapolating it through E_{corr}.

An AutoLab (PGSTAT302N) potentiostat/galvanostat was used to perform the alternating current (AC) impedance spectroscopy measurements. Impedance was measured in the range 100 kHz to 100 MHz with a 1 cm × 1 cm pure iron working electrode embedded in epoxy, Pt as a counter electrode, and an SCE as a reference electrode. The working electrode was initially placed in the test environment for 30 min prior to the impedance run. All experiments were conducted at room temperature. All trials were repeated at least three times to ensure reproducibility and statistical significance of the raw data.

RESULTS AND DISCUSSION

Figure 1 shows the schematic diagram for the fabrication of the SEPI coating. A PDMS prepolymer is first cast against the surface of a fresh *Xanthosoma sagittifolium* leaf and then cured under proper conditions. The prepared PDMS template has negative *Xanthosoma sagittifolium* leaf surface structures and is obtained after peeling off the leaf. The substrate is then covered with the EPAA solution, and the template is pressed against the cold-rolled steel (CRS). After thermal imidization, the PDMS template is peeled off, and a *Xanthosoma sagittifolium*-leaf-like surface is formed on the CRS.

Characterization of EPI. Figure 2 shows the FTIR spectra for the obtained ACAT-based EPAA and EPI materials. In both FTIR spectra, the characteristic peak found at 3340 cm^{-1} was attributed to the N−H stretching modes. Moreover, characteristic peaks at 1600 and 1504 cm^{-1} were designated as the stretching modes of N═Q═N and N−B−N, respectively (Q represents the quinoid ring, and B represents the benzene ring). The characteristic peak at 1373 cm^{-1} was assigned to C═N stretching. The absorption band found at 825 cm^{-1} corresponded to the out-of-plane C−H deformation mode. In the spectrum for the ACAT-based EPAA (Figure 2a), the characteristic peaks for C═O in COOH were found at 1712 cm^{-1}. In the spectrum for the thermally imidized ACAT-based EPAA, vibrational modes were found at 1774 and 1712 cm^{-1}, which may be associated with asymmetric and symmetric carbonyl stretching, respectively. Moreover, the characteristic band found at 740 cm^{-1} was designated as the deformation of the imide groups, as shown in Figure 2(b). The changes in the characteristic peaks in the spectra for the ACAT-based EPAA

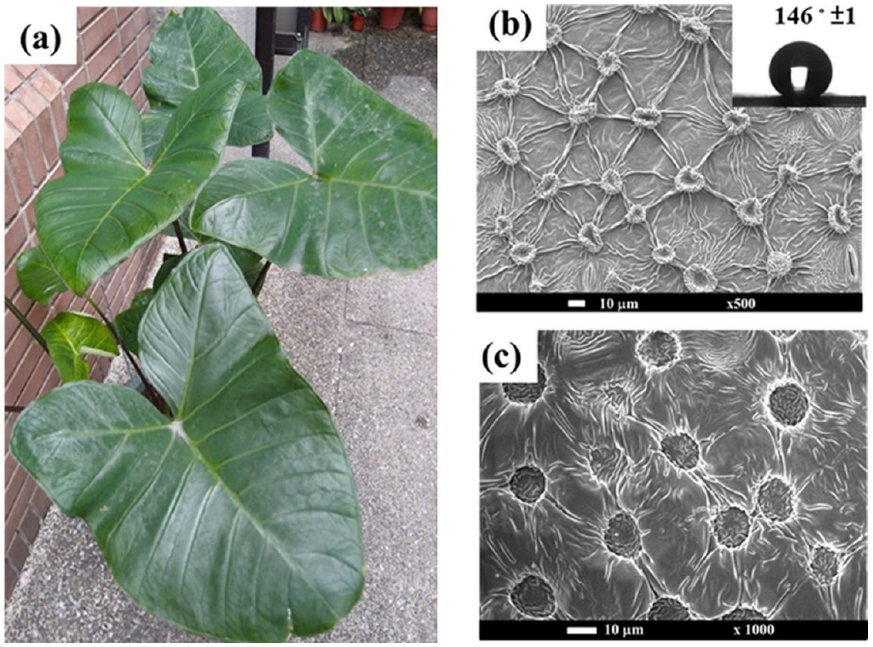

Figure 3. (a) Photograph of *Xanthosoma sagittifolium* leaves. (b) SEM image of fresh, natural leaf. Illustration is water contact angle of *Xanthosoma sagittifolium* leaf. (c) PDMS negative template.

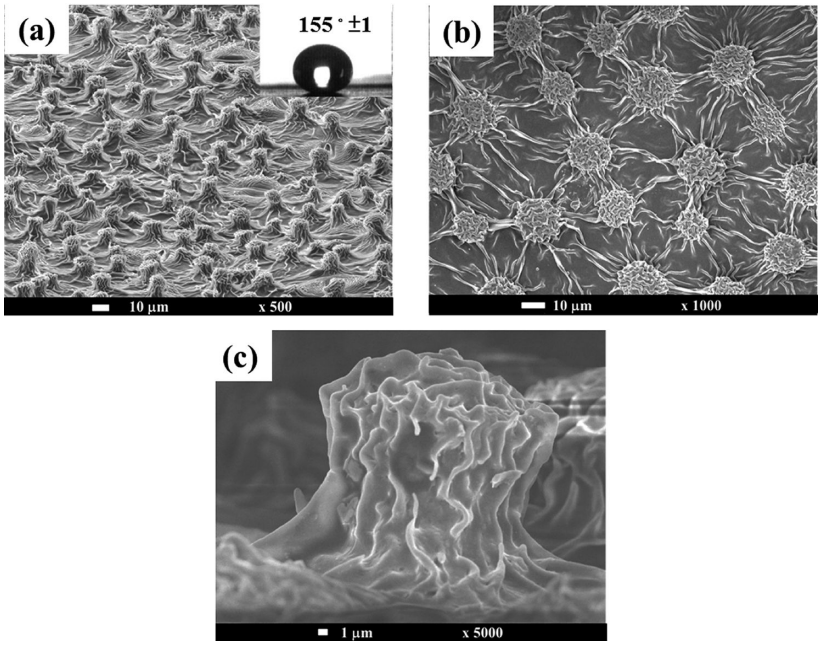

Figure 4. SEM images of (a) *Xanthosoma-sagittifolium*-leaf-like superhydrophobic polymeric surface. Inset shows contact angle of polymeric surface. (b) Topview of polymeric surface. (c) Cross-sectional view of polymeric surface.

and EPI indicate that the EPAA was almost completely converted into the corresponding ACAT-based EPI through thermal imidization at 200 °C.

Microscopic Observations. A photograph of natural, fresh *Xanthosoma sagittifolium* leaves is shown in Figure 3(a). Figure 3(b) is the high magnification SEM image of the *Xanthosoma sagittifolium* leaf. The average contact angle formed on the fresh *Xanthosoma sagittifolium* leaves is *ca.* 146°, as shown in the illustration in Figure 3(b). From Figure 3(b), many small papillary hills are clearly visible on the natural *Xanthosoma sagittifolium* leaf. The diameters of the small papillary hills are between 7 and 9 μm. Figure 3(c) is the SEM image of the PDMS template prepared by casting the liquid PDMS directly onto a natural, fresh *Xanthosoma sagittifolium* leaf. Many holes whose diameters range from 7 to 9 μm are shown on the surface of the PDMS template. Figure 3c shows that the topographic structure of the hole on the surface complements the papillary hills in the natural, fresh *Xanthosoma sagittifolium* leaf. This result demonstrates that the template replicated the topologically inverse structures of the *Xanthosoma sagittifolium* leaf surfaces.

The PDMS templates and nanocasting were used to fabricate the SEPI coating. In this work, EPI was used to prepare the ink. In the past decade, some academic literature has reported that

EPI coatings exhibited better anticorrosion properties[47,48] than several polymers on metallic substrates because the coatings exhibited excellent adhesion, hardness, and chemical resistance.

Figure 4 shows the structures on the surfaces of the nanocasted layers on the CRS slides observed using SEM. Numerous papillary microstructures whose average diameter is about 7−9 μm are formed on the surfaces. The papillary microstructures are replicas of the surface patterns of the *Xanthosoma sagittifolium* leaves.

Contact Angle (Wettability) Measurements. The coating material replicated from the fresh *Xanthosoma sagittifolium* leaves shows superhydrophobic characteristics and a large water contact angle. Figure 5 shows the change in the water contact angle with various times for SEPI. The durability of the water repellent on the SEPI coating is a very important issue. The SEPI was stored at room temperature in the ambient atmosphere for 1 month, and water contact angles were measured under each condition. Almost no decrease in the water contact angle was observed, indicating that the superhydrophobic property of the as-prepared SEPI coating is stable.

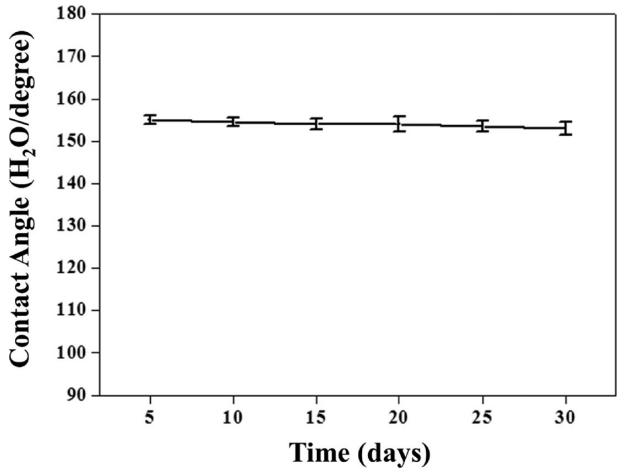

Figure 5. Change in water contact angle for various times for SEPI.

The *Xanthosoma-sagittifolium*-leaf-like-structured EPI coating obviously has a larger water contact angle (*ca.* 155°) than the smooth-surface EPI coating (ca. 87°), as listed in Table 1. As a significant amount of air was trapped between the papillary hills of the EPI surface, a water drop on such a coating could only make contact with the tops of the papillary hills. Thus, the water placed on the surface of the EPI coating was likely resting on a cushion of air.

Table 1. Contact Angle, Surface Properties, And Electrochemical Corrosion Measurements of Bare CRS, EPI, and SEPI-Coated Electrodes

	electrochemical corrosion measurements[a]				
sample code	E_{corr} (mV vs SCE)	R_p (kΩcm^2)	I_{corr} (μA/cm^2)	thickness (μm)	contact angle (deg/H_2O)
CRS	−832	2.00	14.50		84 ± 1
EPI	−553	53.75	1.20	32 ± 2	87 ± 1
SEPI	−452	152.40	0.55	34 ± 2	155 ± 1

[a]Saturated calomel electrode (SCE) was employed as a reference electrode.

It should be noted that the topographic structure on the surface of the CRS complements the papillary hills of the natural, fresh *Xanthosoma sagittifolium* leaf. When various smooth substrates such as glass slides or CRS substrates are used, the resulting surface features are almost identical because they are replicated on a thin layer that completely covers the substrate surfaces. The PDMS template played a key role in replicating highly accurate surface features. Because of its low surface energy and good solidification, the PDMS template could be used to replicate the nanostructures on the surface of the *Xanthosoma sagittifolium* leaf with high fidelity and could be easily peeled off without obviously damagingthe surfaces. During the process, the template remained in close contact with the substrate under pressure, which produced the solid nanostructures after replication.

The ability of a coating to protect metal substrates against corrosion depends on three aspects: (1) sorption of water onto the coating, (2) transport of water throughout the coating, and (3) accessibility of water to the coating/substrate interface. Therefore, it is reasonable to accept that the low-wettability SEPI effectively prevented the water from absorbing onto the substrate surface and therefore exhibited an excellent corrosion resistance in wet environments.

Electroactive Analysis of SEPI Coating. As shown in Figure 6, the voltammogram for the SEPI coating showed a single oxidation peak, which is similar to those shown in the voltammograms for many longer oligomers that undergo two electron transfer.[49] For example, the voltammogram for SEPI showed an oxidation current (I_{ox}) and a reduction current. PANI had previously been reported as an advanced coating material that protected metals against corrosion because of the redox catalytic properties of its conjugated structures that

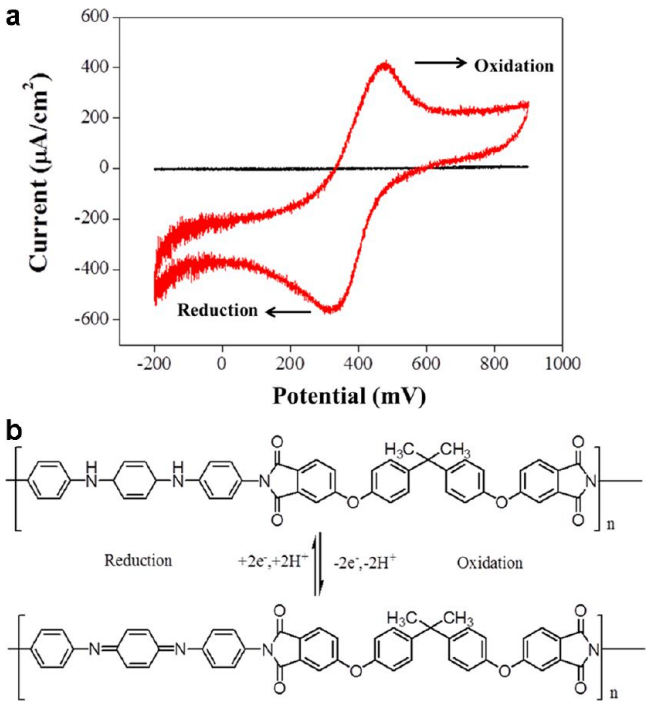

Figure 6. Redox behavior of (a) bare ITO glass and (b) SEPI-coated ITO glass electrode measured in 1.0 M H_2SO_4 aqueous solution.

dx.doi.org/10.1021/am3029377 | ACS Appl. Mater. Interfaces 2013, 5, 1460−1467

induced the formation of a passive layer of metal oxide, resulting in effective protection against corrosion on various metallic surfaces.[3,50] We therefore envisioned that the redox behavior of the as-prepared SEPI coating would probably exhibit an enhanced anticorrosive property similar to that of PANI, as discussed in the following sections.

Potentiodynamic Measurements. On the basis of a series of electrochemical measurements (i.e., corrosion potential, polarization resistance, and corrosion current measured in a corrosive medium (3.5 wt % aqueous NaCl electrolyte)), the SEPI coating was superior at protecting the CRS electrode against corrosion than the EPI coating was because the EPI coating was not superhydrophobic. Information about corrosion current can be obtained by extrapolating Tafel plots, where large cathodic and anodic polarizations provide the cathodic and anodic polarization curves for the respective corrosion processes.[51,52] Extrapolating the cathodic and anodic polarization curves to their point of intersection provides both the corrosion potential and the corrosion current. Corrosion protection studies were performed on samples with 33 ± 1 μm-thick coatings and immersed in a corrosive medium for 30 min. Tafel plots for the two samples immersed in the corrosive medium are shown in Figure 7 and the corresponding data are listed in Table 1.

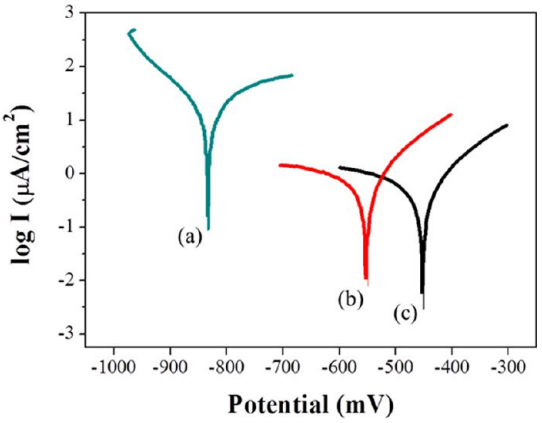

Figure 7. Tafel plots for (a) bare, (b) EPI-coated, and (c) SEPI-coated CRS electrodes measured at 25 ± 0.5 °C.

The Tafel plots for the sample-coated CRS electrode measured at an operational temperature of 25 ± 0.5 °C gave a corrosion potential of E_{corr} = −553 mV for the EPI coating, which was more positive than that for the bare CRS electrode, where E_{corr} = −832 mV. Moreover, the corrosion current (I_{corr}) of the EPI-coated CRS electrode was ca. 1.20 μA/cm^2, which was significantly lower than that of the bare CRS electrode (i.e., 14.50 μA/cm^2).

The corresponding corrosion current (I_{corr}) decreased considerably from 1.20 to 0.55 μA/cm^2 when we used the EPI-coated bare CRS electrode with *Xanthosoma sagittifolium*-leaf-like structures (SEPI) to produce superhydrophobic properties. Moreover, the corrosion potential (E_{corr}) of the SEPI-coated CRS electrode was more positive than that of the EPI-coated CRS electrode. For example, E_{corr} increased from −553 to −452 mV (vs. SCE) for the SEPI-coated CRS electrode. On the basis of the electrochemical measurements, the SEPI coating exhibited protection against corrosion of the CRS electrode.

The SEPI coating exhibited excellent water repellent properties because of the rough morphology similar to small hills on the surface, enabling air to be trapped within the valleys between the hills. Therefore, the neither water nor Cl^- ions in the corrosive medium could readily penetrate the undercoating (such as EPI) of the CRS electrode because of the obstructive effects of the air in the valleys.

The surface morphology, therefore, could indirectly prevent the coating from being reduced by the corrosive medium. Thus, the SEPI-coated CRS electrode resists corrosion better than the bare and EPI-coated CRS electrodes.

Electrochemical Impedance Measurements. "Dielectric spectroscopy," sometimes called "impedance spectroscopy" or "electrochemical impedance spectroscopy" (EIS), is used to measure the dielectric properties of a medium and express them as functions of frequency.[53,54] EIS was also used to examine the difference in the activity between the surface of the bare CRS electrode and the EPI- or SEPI-coated ones. Impedance is a totally complex resistance when a current flows through a circuit consisting of capacitors, resistors, or insulators, or any combination thereof.[55] EIS measurements result in currents produced over a wide range of frequencies. Complex nonlinear least-squares procedures available in numerous EIS-data-fitting computer programs should be used to fit the model to the experimental data in order to obtain the Randles circuit parameters. For simulation studies, corrosive metals are modeled using an equivalent circuit (called a "Randles circuit"), as illustrated in Figure 8, which consists of a double-layer

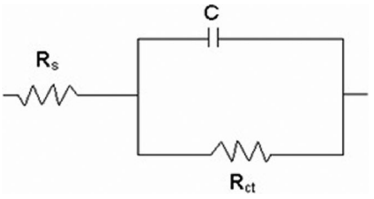

Figure 8. Randles equivalent circuit.

capacitor connected in parallel with a charge-transfer resistor and in series with an electrolyte solution resistor. The impedance (Z) depends on the charge-transfer resistance (R_{ct}), the solution resistance (R_s), the capacitance of the electrical double layer, and the frequency of the AC signal (ω). Z can be deduced as follows:

$$Z = Z' + jZ''$$
$$= R_s + R_{ct}/[1 + (R_{ct}C_{dl}\omega)^2] + j(R_{ct}{}^2C_{dl}\omega)/[1 + (R_{ct}C_{dl}\omega)^2]$$

The fitted data fits well to all the experimental electrochemical data. The high-frequency intercept represents the solution resistance, and the low-frequency intercept represents the sum of the solution and charge-transfer resistances.[33] The larger the diameter of the semicircle (charge-transfer resistance), the lower the corrosion rate.[33,34]

Figure 9 shows the Nyquist plots for the three measured samples. The charge transfer resistances of the bare CRS, EPI-coated, and SEPI-coated electrodes were 1.27, 54.69, and 446.90 kΩ cm^2, respectively. This result clearly demonstrates that the SEPI coating protects the CRS electrode against corrosion better than the EPI coating does. The increase in impedance from a low to a high frequency for the EPI-coated

dx.doi.org/10.1021/am3029377 | ACS Appl. Mater. Interfaces 2013, 5, 1460−1467

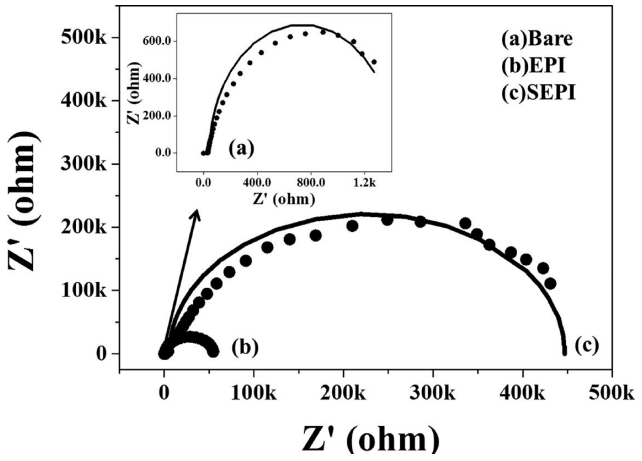

Figure 9. Nyquist plots for (a) bare, (b) EPI-coated, and (c) SEPI-coated CRS electrodes.

electrode can be attributed to the superhydrophobicity of the SEPI coating.

CONCLUSIONS

In conclusion, nanocasting technique was used to prepare a SEPI coating whose surface structure is similar to that of a natural lotus leaf. The morphology of the surface of the as-synthesized SEPI coating showed numerous micromastoids, each decorated with many nanowrinkles. The water contact angle of the SEPI coating whose surface was imprinted with the biomimetic pattern of the surface of a natural leaf was 155°, which was significantly larger than that of the EPI coating (i.e., CA = 87°). We then conducted a series of electrochemical measurements under saline conditions to determine how effective the SEPI coating would be at protecting the CRS electrode against corrosion. The potentiodynamic and electrochemical impedance spectroscopic measurements show that the SEPI coating provides some protection against corrosion of the CRS substrate and provides an effective barrier against aggressive oxidative species. It is believed that this method can be easily applied to the large-scale production of superhydrophobic materials used for commercial corrosion-resistant applications.

AUTHOR INFORMATION

Corresponding Author

*Tel.: +886-3-2653341. Fax: +886-3-2653399. E-mail address: juiming@cycu.edu.tw.

Notes

The authors declare no competing financial interest.

ACKNOWLEDGMENTS

We gratefully acknowledge the financial support of the Ministry of Education (MOE), Taiwan, R.O.C., NSC 101-2113-M-033-005-MY1, the Center-of-Excellence (COE) Program on Membrane Technology from MOE, R.O.C., the Department of Chemistry at Chung Yuan Christian University (CYCU) (CYCU-01RD-RA002-11235), and the Center for Nanotechnology at CYCU.

REFERENCES

(1) Kohlman, R. S.; Joo, J.; Epstein, A. J. Conducting Polymers: Electrical Conductivity. In *Physical Properties of Polymers Handbook*; Mark, J. E., Ed.; AIP Series in Polymers and Complex Materials; American Institute of Physics, Woodbury, NY, 1996.
(2) Trivedi, D. C. Polyanilines. In *Handbook of Organic Conductive Molecules and Polymers*; Nalwa, H. S., Ed.; John Wiley & Sons: New York, 1997; Vol. 2, 505−572.
(3) DeBerry, D. W. *J. Electrochem. Soc.* **1985**, *132*, 1022−1026.
(4) Ahmad, N.; MacDiarmid, A. G. *Synth. Met.* **1996**, *78*, 103−110.
(5) Camalet, J. L.; Lacroix, J. C.; Aeiyach, S.; Chane-Ching, K. I.; Lacaze, P. C. *J. Electroanal. Chem.* **1996**, *416*, 179−182.
(6) Meneguzzi, A.; Lacroix, J. C.; Piro, B.; Adenier, A.; Ferreira, C. A.; Pham, M. C.; Lacaze, P. C. *J. Electrochem. Soc.* **2001**, *148*, B121−B126.
(7) MacDiarmid, A. G.; Mu, S. L.; Somasiri, N. L. D.; Wu, W. *Mol. Cryst. Liq. Cryst.* **1985**, *121*, 187−190.
(8) MacDiarmid, A. G.; Yang, L. S.; Huang, W. S.; Humphrey, B. D. *Synth. Met.* **1987**, *18*, 393−398.
(9) Sivaraman, P.; Hande, V. R.; Mishra, V. S.; Rao, C. S.; Samui, A. B. *J. Power. Sources* **2003**, *124*, 351−354.
(10) Huang, J.; Virji, S.; Weiller, B. H.; Kaner, R. B. *J. Am. Chem. Soc.* **2003**, *125*, 314−315.
(11) Huang, J.; Virji, S.; Weiller, B. H.; Kaner, R. B. *Chem.—Eur. J.* **2004**, *10*, 1314−1319.
(12) Anderson, M. R.; Mattes, B. R.; Reiss, H.; Kaner, R. B. *Science* **1991**, *252*, 1412−1415.
(13) Kaner, R. B. *Synth. Met.* **2001**, *125*, 65−71.
(14) Huang, S. C.; Ball, I. J.; Kaner, R. B. *Macromolecules* **1998**, *31*, 5456−5464.
(15) Trivedi, D. C.; Dhawan, S. K. *Mater. Chem.* **1992**, *2*, 1091−1096.
(16) Maziarz, E. P.; Lorenz, S. A.; White, T. P.; Wood, T. D. *J. Am. Soc. Mass. Spectrom* **2000**, *11*, 659−663.
(17) Taka, T. *Synth. Met.* **1991**, *41*, 1177−1180.
(18) Joo, J.; Epstein, J. *Appl. Phys. Lett.* **1994**, *65*, 2278−2280.
(19) Tao, Y.; Shen, Y.; Yang, L.; Han, B.; Huang, F.; Li, S.; Chu, Z.; Xie, A. *Nanoscale* **2012**, *4*, 3729−3733.
(20) Wang, Y.; Liu, J.; Tran, H. D.; Mecklenburg, M.; Guan, X. N.; Stieg, A. Z.; Regan, B. C.; Martin, D. C.; Kaner, R. B. *J. Am. Chem. Soc.* **2012**, *134*, 9251−9262.
(21) Martin, R. E.; Diederich, F. *Angew. Chem., Int. Ed.* **1999**, *38*, 1351−1377.
(22) Zhou, Y. C.; Geng, J. X.; Li, G.; Zhou, E.; Chen, L.; Zhang, W. J. *J. Polym. Sci., Part B: Polym. Phys.* **2006**, *44*, 764−769.
(23) Singer, R. A.; Sadighi, J. P.; Buchwald, S. L. *J. Am. Chem. Soc.* **1998**, *120*, 213−214.
(24) Wang, Z. Y.; Yang, C.; Gao, J. P.; Lin, J.; Meng, X. S.; Wei, Y.; Li, S. *Macromolecules* **1998**, *31*, 2702−2704.
(25) Lu, W.; Meng, X. S.; Wang, Z. Y. *J. Polym. Sci., Part A: Polym. Chem.* **1999**, *37*, 4295−4301.
(26) Chao, D. M.; Cui, L.; Lu, X. F.; Mao, H.; Zhang, W. J.; Wei, Y. *Eur. Polym. J.* **2007**, *43*, 2641−2647.
(27) Feng, L.; Li, S.; Li, Y.; Li, H.; Zhang, L.; Zhai, J.; Song, Y.; Liu, B.; Jiang, L.; Zhu, D. *Adv. Mater.* **2002**, *14*, 1857−1860.
(28) Erbil, H. Y.; Demirel, A. L.; Avci, Y.; Mert, O. *Science* **2003**, *299*, 1377−1380.
(29) Sun, T.; Feng, L.; Gao, X.; Jiang, L. *Acc. Chem. Res.* **2005**, *38*, 644−652.
(30) Otten, A.; Herminghaus, S. *Langmuir* **2004**, *20*, 2405−2408.
(31) Furstner, R.; Barthlott, W.; Neinhuis, C.; Walzel, P. *Langmuir* **2005**, *21*, 956−961.
(32) Sun, M.; Luo, C.; Xu, L.; Ji, H.; Ouyang, Q.; Yu, D.; Chen, Y. *Langmuir* **2005**, *21*, 8978−8981.
(33) Zhao, X. M.; Xia, Y. N.; Whitesides, G. M. *J. Chem. Mater.* **1997**, *7*, 1069−1074.
(34) Brittain, S.; Paul, K.; Zhao, X. M.; Whitesides, G. *Phys. World* **1998**, *11*, 31−36.
(35) Taguchi, A.; Smatt, J. H.; Linden, M. *Adv. Mater.* **2003**, *15*, 1209−1211.
(36) Qu, M.; Zhao, G.; Cao, X.; Zhang, J. *Langmuir* **2008**, *24*, 4185−4189.
(37) Zhu, Y.; Li, J.; Wan, M.; Jiang, L. *Polymer* **2008**, *49*, 3419−3423.

(38) Xu, L.; Wang, J.; Song, Y.; Jiang, L. *Chem. Mater.* **2009**, *20*, 3554−3556.
(39) Wong, J. Y.; Langer, R.; Ingber, D. E. *Proc. Natl. Acad. Sci. U.S.A.* **1994**, *91*, 3201−3204.
(40) Isaksson, J.; Tengstedt, C.; Fahlman, M.; Robinson, N.; Berggren, M. *Adv. Mater.* **2004**, *16*, 316−320.
(41) Hermelin, E.; Petitjean, J.; Lacroix, J. C.; Chane-Ching, K. I.; Tanguy, J.; Lacaze, P. C. *Chem. Mater.* **2008**, *20*, 4447−4456.
(42) Xu, L.; Chen, W.; Mulchandani, A.; Yan, Y. *Angew. Chem., Int. Ed.* **2005**, *44*, 6009−6012.
(43) Weng, C. J.; Chang, C. H.; Peng, C. W.; Chen, S. W.; Yeh, J. M.; Hsu, C. L.; Wei, Y. *Chem. Mater.* **2011**, *23*, 2075−2083.
(44) Yang, T. I.; Peng, C. W.; Lin, Y. L.; Weng, C. J.; Edgington, G.; Mylonakis, A.; Huang, T. C.; Hsu, C. H.; Yeh, J. M.; Wei, Y. *J. Mater. Chem.* **2012**, *22*, 15845−15852.
(45) Wei, Y.; Yang, C.; Ding, T. *Tetrahedron Lett.* **1996**, *37*, 731−734.
(46) Huang, K. Y.; Shiu, C. L.; Wu, P. S.; Wei, Y.; Yeh, J. M.; Li, W. T. *Electrochim. Acta* **2009**, *54*, 5400−5407.
(47) Huang, K. Y.; Jhuo, Y. S.; Wu, P. S.; Lin, C. H.; Yu, Y. H.; Yeh, J. M. *Eur. Polym. J.* **2009**, *45*, 485−493.
(48) Huang, T. C.; Yeh, T. C.; Huang, H. Y.; Ji, W. F.; Chou, Y. C.; Hung, W. I.; Yeh, J. M.; Tsai, M. H. *Electrochim. Acta* **2011**, *56*, 10151−10158.
(49) Chen, R.; Benicewicz, B. C. *Macromolecules* **2003**, *36*, 6333−6339.
(50) Wessling, B.; Posdorfer, J. *Synth. Met.* **1999**, *102*, 1400−1401.
(51) Mitra, A.; Wang, Z. B.; Cao, T. G.; Wang, H. T.; Huang, L. M.; Yan, Y. S. *J. Electrochem. Soc.* **2002**, *149*, B472−B478.
(52) Beving, D. E.; McDonnell, A. M. P.; Yang, W. S.; Yan, Y. S. *J. Electrochem. Soc.* **2006**, *153*, B325−B329.
(53) Liu, Y. D.; Fang, F. F.; Choi, H. J. *Langmuir* **2010**, *26*, 12849−12854.
(54) Liu, Y. D.; Park, B. J.; Kim, Y. H.; Choi, H. J. *J. Mater. Chem.* **2011**, *21*, 17396−17402.
(55) Park, S. M.; Yoo, J. S. *Anal. Chem.* **2003**, *21*, 455A−461A.